

Theory of spin-orbit enhanced electric-field control of magnetism in multiferroic BiFeO_3

Rogério de Sousa* and Marc Allen

Department of Physics and Astronomy, University of Victoria, Victoria, B.C., V8W 3P6, Canada

Maximilien Cazayous

*Laboratoire Matériaux et Phénomènes Quantiques (UMR 7162 CNRS),
Université Paris Diderot-Paris 7, 75205 Paris cedex 13, France*

(Dated: October 1, 2012)

We present a microscopic theory that shows the importance of spin-orbit coupling in multiferroic compounds with heavy ions. In BiFeO_3 (BFO) the spin-orbit coupling at the bismuth ion sites results in a special kind of magnetic anisotropy that is linear in the applied E -field. We show how this interaction is capable of disrupting the magnetic cycloid state of bulk BFO, leading to a remarkable level of E -field control of magnetism.

PACS numbers: 75.85.+t, 71.70.Ej, 75.30.Gw, 77.80.Fm

The ability to control magnetism using electric fields is of great fundamental and practical interest. It may allow the development of ideal magnetic memories with electric write and magnetic read capabilities [1], as well as logic devices based on spin waves that dissipate much less energy [2]. Usually, the interactions that couple spin to electric degrees of freedom are too weak to induce qualitative changes to magnetic states. Hence, the search for enhanced couplings has focused on multiferroic materials with coexisting magnetic and ferroelectric phases [3].

The key physical interaction that enables cross correlation between electric and magnetic degrees of freedom is the linear magnetoelectric effect (LME). It occurs when the coupling between spin and charge is linear in either the external electric field \mathbf{E} or the internal polarization \mathbf{P} , and is quadratic in electron spin. In a large class of multiferroic materials, the dominant form of LME was found to be due to the spin-current effect [4], that couples localized spins according to $\mathcal{H}_{\text{SC}} = \sum_{i < j} J_{\text{SC}}(\mathbf{P} \times \mathbf{R}_{ij}) \cdot (\mathbf{S}_i \times \mathbf{S}_j)$, with \mathbf{R}_{ij} the vector linking the atomic location of spin \mathbf{S}_i to the atomic location of spin \mathbf{S}_j . In manganese-based multiferroics, the spin-current interaction leads to magnetic induced ferroelectricity and thus allows magnetic field control of ferroelectricity [5].

For E -field control of magnetism, research has been centered instead on iron-based multiferroics, with bismuth ferrite [BiFeO_3 or BFO] being the most notable example [6]. At temperatures below 1143 K, BFO develops a strong electric polarization $P = 100 \mu\text{C}/\text{cm}^2$ that points along one of the eight cube diagonals of its unit cell [Fig. 1(a)]. It becomes an antiferromagnet below 643 K with Fe spins forming a spiral of the cycloid type, described by antiferromagnetic Néel vector $\hat{\mathbf{L}} = \sin(\mathbf{q} \cdot \mathbf{r})\hat{\mathbf{q}} + \cos(\mathbf{q} \cdot \mathbf{r})\hat{\mathbf{P}}$. The microscopic origin of the cycloid can also be understood as arising from the spin-current interaction [7]. Plugging the cycloid \mathbf{L} into \mathcal{H}_{SC} , one finds that the lowest energy state is always

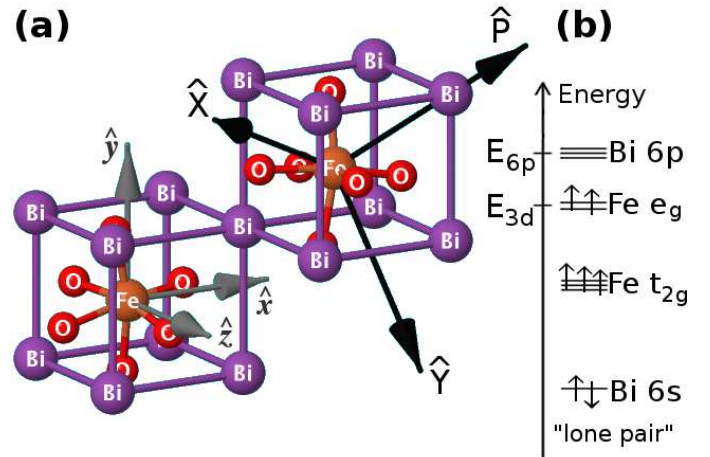


FIG. 1: (color online) (a) Conventional unit cell for BFO. The simple cubic axis \hat{x} , \hat{y} , \hat{z} are denoted by grey vectors. The ferroelectric polarization \mathbf{P} is shown pointing along [111], arising mostly from the displacement of Bi ions with respect to the oxygens. The directions \hat{X} and \hat{Y} denoted by black vectors describe the plane perpendicular to \mathbf{P} [10]. (b) Energy level diagram for $\text{Fe}^{3+} = [\text{Ar}]3d^5$ and $\text{Bi}^{3+} = [\text{Pt}]6s^2$ orbitals in BFO; the Fermi level lies just above E_{3d} .

achieved when the cycloid wavevector \mathbf{q} is perpendicular to \mathbf{P} . Hence the spins are pinned to the plane formed by \mathbf{P} and \mathbf{q} . This fact has been central to all demonstrations of E -field control of magnetism published to date; the application of an E -field poles \mathbf{P} from one cube diagonal to another, forcing the spin cycloidal arrangement to move into another plane [8, 9].

A recent experiment [2] suggested that the spin-current interaction is not the only LME present in BFO. The application of an external E -field to bulk BFO was shown to result in a giant shift of magnon frequencies that was linear in \mathbf{E} and 10^5 times larger than any other known

E -field effect on magnon spectra.

In this letter, we present a microscopic theory of E -field induced magnetic anisotropy, and argue that it can provide an effective source of LME in magnetoelectric materials with large spin-orbit coupling. Our predicted LME explains the origin of the E -field effect on magnon spectra measured in bulk BFO [2]. Moreover, we show that this effect is capable of qualitatively changing the cycloidal spin state of BFO, leading to homogeneous magnetism with orientation controllable by the direction of the applied E -field.

Model and microscopic calculation of LME.—Our microscopic Hamiltonian for coupling between spin and electric-field has three contributions, $\mathcal{H} = \mathcal{H}_{\text{latt}} + \mathcal{H}_{\text{orb}} + \mathcal{H}_{\text{SO}}$. The first term is due to the lattice potential, $\mathcal{H}_{\text{latt}} = -\hbar^2 \nabla^2 / (2m_e) + V_{\text{crystal}}(\mathbf{r})$, with m_e the free electron mass. The second term is called an orbital term and is given by $\mathcal{H}_{\text{orb}} = -e\mathbf{r} \cdot \mathbf{E}$, with $e < 0$ and \mathbf{r} the electron's charge and coordinate, respectively. The last and most important term is the spin-orbit interaction, $\mathcal{H}_{\text{SO}} = \zeta \boldsymbol{\ell} \cdot \boldsymbol{\sigma}$, with $\boldsymbol{\ell} = -i\mathbf{r} \times \nabla$ the electron's orbital angular momentum and $\boldsymbol{\sigma}$ its spin operator. We take the spin-orbit interaction to be dominated by the heaviest ion of the lattice, and take bismuth in BFO as a prototypical example.

Single ion anisotropy is known to arise as a correction to the total spin energy that is second order in the spin-orbit interaction [11]. In our case the largest contribution arises in the fourth order of our total Hamiltonian, i.e., second order in \mathcal{H}_{SO} and second order in $\mathcal{H}_{\text{latt}}$ or \mathcal{H}_{orb} . An explicit calculation yields

$$\mathcal{H}_{\text{SIA}} = -\frac{1}{(2S)^2} \mathbf{S} \cdot \left[\sum_{m,n} \frac{\mathbf{V}_{mn} \otimes \mathbf{V}_{nm}}{E_{6p} - E_{3d_m}} \right] \cdot \mathbf{S}, \quad (1)$$

where the spin operator $\mathbf{S} = \sum_{i=1}^5 \boldsymbol{\sigma}_i$ represents all five electron spins in the Fe^{3+} d-shell. The numerator of Eq. (1) is an outer product between vectors

$$\mathbf{V}_{mn} = - \sum_{n', \mathbf{R}_{\text{Bi}}} \frac{\langle 3d_m | \mathcal{H}_{\text{latt, orb}} | 6p_{n'} \rangle \langle 6p_{n'} | \zeta \boldsymbol{\ell} | 6p_n \rangle}{E_{6p} - E_{3d_m}}, \quad (2)$$

involving 6p and 3d localized orbitals at Bi and Fe, respectively, with a sum over all vectors \mathbf{R}_{Bi} linking the central Fe to each of its eight neighboring Bi. We evaluate Eq. (2) by taking as Bi orbitals the states $|6p_x\rangle$, $|6p_y\rangle$, $|6p_z\rangle$, and as Fe orbitals the e_g states $|3d_{3z^2-r^2}\rangle$ and $|3d_{x^2-y^2}\rangle$, written with respect to the cubic axis $\hat{\mathbf{x}}, \hat{\mathbf{y}}, \hat{\mathbf{z}}$ of BFO's parent perovskite lattice. The Fe t_{2g} states need not be considered because they are ≈ 5 eV lower in energy [11], and only give a small correction to Eq. (1).

We now turn to an explicit evaluation of the matrix elements appearing in Eq. (2). The spin-orbit matrix element is given by

$$\langle 6p_{n'} | \zeta \boldsymbol{\ell} | 6p_n \rangle = -i\eta \hat{\mathbf{n}}' \times \hat{\mathbf{n}}, \quad (3)$$

with $\eta = 0.86$ eV chosen to match the spin-orbit splitting measured in isolated Bi ions [12]. Using symmetry,

all lattice matrix elements $\langle 3d_m | \mathcal{H}_{\text{latt}} | 6p_{n'} \rangle$ can be expressed in terms of the direction cosines of \mathbf{R}_{Bi} plus only two parameters: $V_{pd\sigma} = \langle 3d_{3z^2-r^2} | \mathcal{H}_{\text{latt}} | 6p_{z'} \rangle$ and $V_{pd\pi} = \langle 3d_{x'^2-z'^2} | \mathcal{H}_{\text{latt}} | 6p_{x'} \rangle$, with z' pointing along \mathbf{R}_{Bi} . A similar procedure can be applied to the orbital matrix elements $\langle 3d_m | \mathcal{H}_{\text{orb}} | 6p_{n'} \rangle$, reducing them to expressions that depend on the direction cosines of \mathbf{R}_{Bi} plus matrix elements like $\langle 3d_{x'z'} | z' | 6p_{x'} \rangle$, etc.

In order to compute the vectors in Eq. (2), we need to sum over all Bi neighbors forming a distorted cube around each Fe. We do this by converting the sum into an angular integral,

$$\sum_{\mathbf{R}_{\text{Bi}}} \langle 3d_m | \mathcal{H}_{\text{latt, orb}} | 6p_{n'} \rangle \approx \frac{8}{4\pi} \int d\Omega_{\mathbf{R}} [1 + \delta\mathbf{R} \cdot \nabla_{\mathbf{R}}] \times \langle 3d_m | \mathcal{H}_{\text{latt, orb}} | 6p_{n'} \rangle, \quad (4)$$

with $\delta\mathbf{R} = (R_{\parallel} \hat{\mathbf{P}} + u_{\perp} \mathbf{E}_{\perp})$ denoting the deviation of the Bi ions from the perfect cube. This includes Bi displacement along $\hat{\mathbf{P}}$ causing ferroelectricity; the displacement is given by $R_{\parallel} = 0.116 R_{\text{Bi}}$ with $R_{\text{Bi}} = 4.88 \text{ \AA}$ [16]. The component of \mathbf{E} along $\hat{\mathbf{P}}$ can be neglected (it can not compete with the internal field generated by ferroelectricity), so we write the external E -field as $\mathbf{E}_{\perp} = E_{\perp} [\cos(\psi) \hat{\mathbf{X}} + \sin(\psi) \hat{\mathbf{Y}}]$, with the rhombohedral axis $\hat{\mathbf{X}}$ and $\hat{\mathbf{Y}}$ shown in Fig. 1(a). This perpendicular component induces additional lattice displacement $u_{\perp} \mathbf{E}_{\perp}$; an estimate based on infrared spectroscopy [14] yields $u_{\perp} \mathbf{E}_{\perp} / R_{\text{Bi}} = 2.4 \times 10^{-4} E_{\perp} / (10^5 \text{ V/cm})$.

After computing the averages over all matrix elements we evaluate the magnetic anisotropy [Eq. (1)] to give rise to two terms:

$$\mathcal{H}_2 = -\frac{a}{2} (\mathbf{S} \cdot \hat{\mathbf{P}})^2, \quad (5)$$

$$\mathcal{H}_E = \frac{(\xi E_{\perp})}{2} \left[\cos(\psi) S_x^2 + \cos\left(\psi - \frac{2\pi}{3}\right) S_y^2 + \cos\left(\psi - \frac{4\pi}{3}\right) S_z^2 \right]. \quad (6)$$

Equation (6) depends linearly on E_{\perp} , i.e., it gives rise to the LME.

Even in the absence of an external E -field, we find a magnetic anisotropy,

$$a = \frac{1792\eta^2}{9(2S)^2} \frac{V_{\parallel}^2}{(E_{6p} - E_{3d})^3}, \quad (7)$$

with a coupling energy related to the lack of inversion symmetry along \mathbf{P} ,

$$V_{\parallel} = \frac{R_{\parallel}}{R_{\text{Bi}}} \left(V_{pd\sigma} + \frac{V_{pd\pi}}{\sqrt{3}} \right). \quad (8)$$

Taking $(E_{6p} - E_{3d})$ to be equal to BFO's band gap of 2.8 eV [15], and using the tabulated values for the Fe-Bi bond $V_{pd\sigma} = -71$ meV and $V_{pd\pi} = -41$ meV [13], we get $V_{\parallel} = -11$ meV and $a = 32 \mu\text{eV} \doteq 0.4$ K.

The effect of the external E -field is to introduce magnetoelectric coupling with reduced symmetry; from Eq. (2) we separate orbital and lattice contributions. The orbital LME is given by

$$\xi_{\text{orb}} = \frac{8}{35} \left(\frac{a}{V_{\parallel}} \right) e \left(\langle 3d_{3z^2-r^2} | z' | 6p_{z'} \rangle + \sqrt{3} \langle 3d_{x'z'} | z' | 6p_{x'} \rangle + 3\sqrt{3} \langle 3d_{y'z'} | y' | 6p_{z'} \rangle + \frac{5}{\sqrt{3}} \langle 3d_{x'y'} | y' | 6p_{x'} \rangle \right. \\ \left. - \langle 3d_{3z^2-r^2} | x' | 6p_{x'} \rangle + \frac{1}{\sqrt{3}} \langle 3d_{x'r^2-y'^2} | x' | 6p_{x'} \rangle \right), \quad (9)$$

while the lattice LME is

$$\xi_{\text{latt}} = -\frac{4\sqrt{2}}{7} \left(\frac{a}{V_{\parallel}} \right) \left(V_{pd\sigma} + \frac{V_{pd\pi}}{\sqrt{3}} \right) \left(\frac{u_{\perp}}{R_{\text{Bi}}} \right). \quad (10)$$

Note how these are physically distinct mechanisms: The lattice mechanism is proportional to $u_{\perp} E_{\perp}$, i.e., it arises from E -field induced lattice displacement contained in $\mathcal{H}_{\text{latt}}$. Plugging the tabulated values for $V_{pd\sigma}$ and $V_{pd\pi}$ we get $\xi_{\text{latt}} = -5 \times 10^{-2} \mu\text{eV}/(10^5 \text{V}/\text{cm})$. The orbital mechanism is instead related to E -field induced orbital admixture, and its matrix elements are not tabulated. Assuming $\langle 3d | x'_i | 6p \rangle \sim R_{\text{Bi}}$ we get an order of magnitude estimate of $\xi_{\text{orb}} \sim +30 \mu\text{eV}/(10^5 \text{V}/\text{cm})$.

Comparison to experiments.—The experiment in Ref. [2] discovered a strong dependence of magnon frequencies on the external E -field, and used group theory to fit two kinds of E -field induced anisotropy: These were $F_1 = -(\xi/4)(\mathbf{E}_{\perp} \cdot \mathbf{S})(\mathbf{S} \cdot \hat{\mathbf{P}})$, and $F_2 = -(\xi/4)\mathbf{E}_{\perp} \cdot [(S_Y^2 - S_X^2)\hat{\mathbf{X}} + (2S_X S_Y)\hat{\mathbf{Y}}]$. It was shown that only F_2 would give rise to the observed linear in E_{\perp} magnon shift, and a fit of $\xi_{\text{exp}} = +55 \mu\text{eV}/(10^5 \text{V}/\text{cm})$ with $a = 0$ was established at $T = 300$ K. To compare this result to our theory, we write our Eq. (6) in the rhombohedral basis and get that it is equal to $F_2 + 2\sqrt{2}F_1$. Thus our Eq. (6) can be expressed as a function of the two anisotropy terms of Ref. [2] and explains the origin of the interaction leading to electrical control of magnons in BFO.

Our calculated zero-field anisotropy energy $a = 32 \mu\text{eV}$ is close to the value of $a \approx 20 \mu\text{eV}$ extracted from neutron diffraction experiments [17].

Electric-field control of magnetism.—To find out whether our effect can be used to control magnetism using an external E -field, we incorporate Eq. (6) into the usual continuum free energy model for BFO [18–20],

$$\mathcal{F} = \int d^3x \left\{ -\frac{m'}{2} L^2 + \frac{c'}{2} \sum_{\gamma=x,y,z} |\nabla L_{\gamma}|^2 \right. \\ \left. - \alpha' \mathbf{P} \cdot [\mathbf{L}(\nabla \cdot \mathbf{L}) + \mathbf{L} \times (\nabla \times \mathbf{L})] \right. \\ \left. + \frac{(\xi' E_{\perp})}{2} \left[\cos(\psi) L_x^2 + \cos\left(\psi - \frac{2\pi}{3}\right) L_y^2 \right. \right. \\ \left. \left. + \cos\left(\psi - \frac{4\pi}{3}\right) L_z^2 \right] \right\}. \quad (11)$$

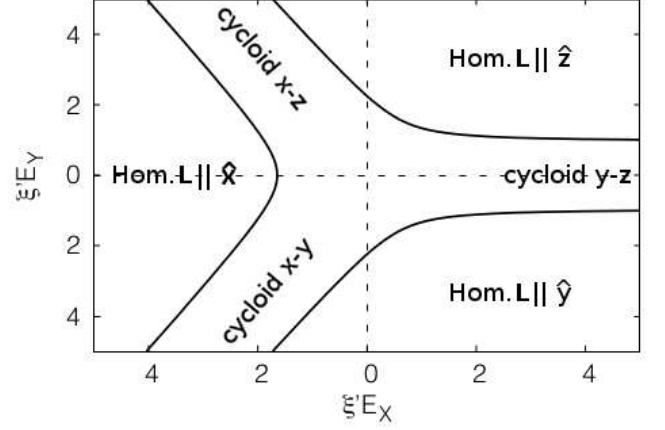


FIG. 2: Electric-field induced magnetic phase diagram for BFO. Here E_X and E_Y are projections of the external E -field in the plane perpendicular to \mathbf{P} ; the axis $\hat{\mathbf{X}}$, $\hat{\mathbf{Y}}$ are shown in Fig. 1(a). A transition from cycloid to homogeneous magnetism is predicted for certain directions in the $X - Y$ plane. In this case the Néel vector \mathbf{L} will point along one of the conventional cubic directions $\hat{\mathbf{n}} = \hat{\mathbf{x}}, \hat{\mathbf{y}}, \hat{\mathbf{z}}$, and due to the Dzyaloshinskii-Moriya coupling the magnetization \mathbf{M} will point along $\hat{\mathbf{P}} \times \mathbf{L}$. Thus an external E -field is able to control the direction of the two magnetic order parameters \mathbf{M} and \mathbf{L} .

Here \mathbf{L} is the Néel vector, and the first and second terms inside the brackets of Eq. (11) arise from the exchange interaction between spins; the third term arises from the continuum limit of the spin-current coupling, leading to $\alpha' = J_{\text{SC}}(\Omega_0/2)^{5/3}/(2S\mu_B)^2$, with $\Omega_0 = 124.32 \text{ \AA}^3$ the unit cell volume in BFO. This term is often called the flexoelectric interaction, and explains the origin of the cycloid in BFO when $c'q^2 \approx 1$ [18, 20]. The fourth term is the continuum limit of Eq. (6), with $2\xi' = (\Omega_0\xi)/(2S\mu_B)^2$.

The minimum free energy state $\mathbf{L}(\mathbf{r})$ can be found using functional derivatives in the same way as done in Refs. [18, 19]. The result is summarized in Fig. 2. As the electric field is increased, the anisotropy energy favors an anharmonic cycloid ground state with \mathbf{L} forming a square wave along one of the three cubic directions $\hat{\mathbf{x}}, \hat{\mathbf{y}}$, or $\hat{\mathbf{z}}$, depending on the direction of \mathbf{E}_{\perp} . When E_{\perp} be-

comes larger than a certain critical value, we get a phase transition to a homogeneous \mathbf{L} , effectively destroying the cycloid state. The origin of this phase transition is the competition between E -field induced anisotropy and the flexoelectric interaction. The free energy of the cycloid state is $\mathcal{F}_{\text{cycloid}} \approx -(\xi' E_{\perp}/2)\langle \cos^2(\mathbf{q} \cdot \mathbf{r}) \rangle - c'q^2/2 = -\xi' E_{\perp}/4 - c'q^2/2$. Compare this to the free energy of the homogeneous state, $\mathcal{F}_{\text{Hom}} \approx -\xi' E_{\perp}/2$; as E_{\perp} increases, eventually we will have $\xi' E_{\perp} > 2c'q^2$ and $\mathcal{F}_{\text{Hom}} < \mathcal{F}_{\text{cycloid}}$, inducing a transition to the homogeneous state. A detailed calculation yields the following critical field:

$$(\xi' E_{\perp})_c = \frac{\pi^2}{6} (c'q^2) \left[\sin\left(\psi + \frac{\pi}{6}\right) + \left| \frac{\cos\left(\psi + \frac{\pi}{6}\right)}{\tan\left(\frac{3\psi}{2}\right)} \right| \right], \quad (12)$$

for $0 \leq \psi \leq 120^\circ$, and similar expressions for $\psi \rightarrow \psi - 120^\circ$ and $\psi \rightarrow \psi - 240^\circ$. Remarkably, the critical field is infinite when \mathbf{E} points antiparallel to one of the cubic directions. This is also easy to understand from the symmetry of Eq. (6): for example, when \mathbf{E}_{\perp} points along the projection of $-\hat{\mathbf{x}}$ in the $X - Y$ plane ($\psi = 0^\circ$), the electric field anisotropy energy is the same for \mathbf{L} along $\hat{\mathbf{y}}$ or $\hat{\mathbf{z}}$; thus when \mathbf{L} is a cycloid in the $y - z$ plane, it is able to simultaneously minimize both the E -field anisotropy and the flexoelectric energies; in this situation it is energetically favorable for \mathbf{L} to remain a cycloid. A similar situation applies for $\mathbf{E} \parallel -\hat{\mathbf{y}}$ or $\mathbf{E} \parallel -\hat{\mathbf{z}}$.

An important point is that \mathbf{P} can be poled by the external E -field, changing the effective direction of E_{\perp} in Fig. 2 (note that Fig. 2 assumes $\mathbf{P} \parallel [111]$ at all magnitudes of E_{\perp}). To avoid poling, one can apply the E -field with a component along the $[111]$ direction. For example, using $\mathbf{E} = E[\cos(30^\circ)\hat{\mathbf{Z}} - \sin(30^\circ)\hat{\mathbf{X}}]$ allows control of magnetism without changing \mathbf{P} , at the expense of having $E_{\perp} = E/2$. Using $\xi_{\text{exp}} = 55 \mu\text{eV}/(10^5 \text{V}/\text{cm})$ we get that a minimum $E = 1.3 \times 10^5 \text{V}/\text{cm}$ is required to induce the homogeneous state, a value well into the practical range. To confirm our theory we propose the application of the E -field to bulk BFO along this specific direction. The homogeneous state has as its optical signature the presence of only two magnon Raman modes [21] (the signature of the simple antiferromagnet) instead of five or more cyclonic magnons [22].

The ability to switch from cycloidal to homogeneous spin order by way of an external E -field represents a significant step towards the development of spin-based technologies. It enables the engineering of logic gates with magnetic excitations. In addition, BFO is known to have a weak magnetization $\mathbf{M} \propto \hat{\mathbf{Z}} \times \mathbf{L}$ that is generated by the Dzyaloshinskii-Moriya interaction [23, 24], of magnitude $|\mathbf{M}| = 0.06\mu_B/\text{Fe}$ [25]. Since the direction of \mathbf{M} is tied to \mathbf{L} , our mechanism allows E -field control of \mathbf{M} , a functionality that will be useful for the design of magnetic memories that dissipate less energy [1].

Conclusions.—We presented a microscopic theory of E -field induced magnetic anisotropy, and showed how it gives rise to an additional linear magnetoelectric effect (LME) in multiferroic materials. The origin of this special kind of LME is based on the combination of two factors: The presence of a non-magnetic ion with large spin-orbit coupling, and a significant amount of inversion asymmetry (induced e.g. by ferroelectricity). For BFO, the presence of this additional LME implies that its magnetic cycloid can be converted into a homogeneous state under the application of a practical external E -field. Thus, it shows that E -field control of magnetism in BFO can be much more complete than what has been demonstrated so far.

Our research was supported by the NSERC Discovery program.

* rdesousa@uvic.ca

- [1] J.F. Scott, *Nature Mater.* **6**, 256 (2007).
- [2] P. Rovillain, R. de Sousa, Y. Gallais, A. Sacuto, M.A. Méasson, D. Colson, A. Forget, M. Bibes, A. Barthélémy, and M. Cazayous, *Nature Mater.* **9**, 975 (2010).
- [3] See e.g. N.A. Spaldin, S.-W. Cheong, and R. Ramesh, *Phys. Today* **63**, 38 (2010); S.-W. Chong and M. Mostovoy, *Nature Mater.* **6**, 13 (2007).
- [4] H. Katsura, N. Nagaosa, and A.V. Balatsky, *Phys. Rev. Lett.* **95**, 057205 (2005).
- [5] T. Kimura, T. Goto, H. Shintani, K. Ishizaka, T. Arima, and Y. Tokura, *Nature* **426**, 55 (2003).
- [6] G. Catalan and J.F. Scott, *Adv. Mater.* **21**, 2463, (2009); A.M. Kadomtseva, A.K. Zvezdin, Yu.F. Popov, A.P. Pyatakov, and G.P. Vorob'ev, *JETP Lett.* **79**, 571 (2004).
- [7] D. Rahmedov, D. Wang, J. Íñiguez, and L. Bellaiche, *Phys. Rev. Lett.* **109**, 037207 (2012).
- [8] T. Zhao *et al.*, *Nature Mater.* **5**, 823 (2006); Y.-H. Chu *et al.* *Nature Mater.* **7**, 478 (2008).
- [9] D. Lebeugle, D. Colson, A. Forget, M. Viret, A.M. Bataille, and A. Goukasov, *Phys. Rev. Lett.* **100**, 227602 (2008).
- [10] We used the definition $\hat{\mathbf{X}} = (-2\hat{\mathbf{x}} + \hat{\mathbf{y}} + \hat{\mathbf{z}})/\sqrt{6}$ and $\hat{\mathbf{Y}} = (-\hat{\mathbf{y}} + \hat{\mathbf{z}})/\sqrt{2}$ as new rhombohedral axis perpendicular to $\hat{\mathbf{P}} = \hat{\mathbf{Z}} = (\hat{\mathbf{x}} + \hat{\mathbf{y}} + \hat{\mathbf{z}})/\sqrt{3}$.
- [11] See A. Abragam and B. Bleaney, *Electron paramagnetic resonance of transition metal ions* (Clarendon Press, Oxford, U.K., 1970), Chapters 7 and 19.
- [12] The spin-orbit interaction splits the 6p manifold into $j = 3/2$ and $j = 1/2$ levels, with splitting given by 3η . Spectroscopy measurements yield $3\eta = 2.58 \text{ eV}$. See the first excited state of Bi III in the NIST atomic spectra database, <http://physics.nist.gov/asd>.
- [13] W.A. Harrison, *Elementary electronic structure* (World Scientific, Singapore, 2004). The method to calculate matrix elements between localized atomic orbitals is described in p. 546, with tabulated values shown at the end of the book "solid-state table".
- [14] R.P.S.M. Lobo, R.L. Moreira, D. Lebeugle, and D. Colson, *Phys. Rev. B* **76**, 172105 (2007).
- [15] A. Kumar *et al.*, *Appl. Phys. Lett.* **92**, 121915 (2008).

- [16] F. Kubel and H. Schmid, *Acta Crystallogr. Sect. B: Struct. Sci* **46**, 698 (1990).
- [17] M. Ramazanoglu, W. Ratcliff, Y.J. Choi, S. Lee, S.W. Cheong, and V. Kiryukhin, *Phys. Rev. B* **83**, 174434 (2011).
- [18] A. Sparavigna, A. Strigazzi, and A. Zvezdin, *Phys. Rev. B* **50**, 2953 (1994).
- [19] R. de Sousa and J.E. Moore, *Phys. Rev. B* **77**, 012406 (2008).
- [20] I. Sosnowska and A.L. Zvezdin, *J. Magn. Magn. Mater.* **140-144**, 167 (1995).
- [21] R. de Sousa and J.E. Moore, *Appl. Phys. Lett.* **92**, 022514 (2008).
- [22] M. Cazayous, Y. Gallais, A. Sacuto, R. de Sousa, D. Lebeugle and D. Colson, *Phys. Rev. Lett.* **101**, 037601 (2008).
- [23] C. Ederer and N.A. Spaldin, *Phys. Rev. B* **71**, 060401(R) (2005).
- [24] R. de Sousa and J.E. Moore, *Phys. Rev. Lett.* **102**, 249701 (2009).
- [25] M. Ramazanoglu, M. Laver, W. Ratcliff, S. M. Watson, W. C. Chen, A. Jackson, K. Kothapalli, S. Lee, S.-W. Cheong, and V. Kiryukhin, *Phys. Rev. Lett.* **107**, 207206 (2011).